Applied Thermal Engineering 287 (2026) 129446

Contents lists available at ScienceDirect

Applied Thermal Engineering

journal homepage: www.elsevier.com/locate/apthermeng

Research Paper

Performance optimization of a three-stage cascade refrigeration system using response surface methodology

Oguzhan Pektezel [a], Safiye Nur Ozdemir [b,*]

[a] Department of Mechanical Engineering, University of Balikesir, 10145 Balikesir, Turkey
[b] Department of Mechanical Engineering, University of Sakarya, 54050 Adapazari, Turkey

ARTICLE INFO

Keywords:
Three-stage cascade refrigeration system
Ultra-low temperature
Response surface methodology
Multi-objective optimization
Desirability approach

ABSTRACT

Ultra-low-temperature refrigeration is an essential criterion for cryogenic applications, biomedical preservation, and vaccine storage. Three-stage cascade refrigeration system is a conventional solution generally preferred for applications requiring temperatures below −80 °C. In this study, a detailed thermodynamic model was created using the Engineering Equation Solver (EES), and performance optimization was carried out using Response Surface Methodology (RSM) based on a Central Composite Design (CCD) that included 30 experimental runs. The evaporator and condenser temperatures at the low-, medium-, and high-temperature stages were treated as independent decision variables, whereas the coefficient of performance (COP), exergy efficiency (η_{ex}), total exergy destruction ($\dot{E}_{dest}$), and total compressor power (P_{comp}) served as the primary performance responses. The results indicated that the system achieved its optimal thermodynamic performance with an evaporator temperature of −90.043 °C and condenser temperatures of −56.411 °C, −10.941 °C, and 26.077 °C for the low, medium, and high-temperature cycles, respectively. Specifically, the maximum COP was recorded at 0.697, while the highest exergy efficiency reached 41.4 %. The total exergy destruction and compressor power consumption were also minimized to 5.545 kW and 11.394 kW, respectively. The main contribution of this study is employing RSM to systematically optimize the operating parameters of a conventional three-stage cascade cycle. By integrating RSM with detailed thermodynamic analysis, this study provides an optimization framework that can guide the design and operation of low-temperature cascade refrigeration systems.

1. Introduction

According to ASHRAE, refrigeration systems operating at temperatures below −50 °C fall into the category of ultra-low temperature refrigeration. A range of applications—including scientific experimentation in low-temperature environments, organ preservation, and the production of specialty foods—necessitate operating at temperatures below −50 °C [1]. The emergence of the need for −80 °C storage units to preserve vaccines required for combating the COVID-19 pandemic has once again highlighted the importance of ultra-low temperature refrigeration systems in recent years. In addition, ultra-low temperatures are required in various industrial processes such as natural gas liquefaction, petroleum gas liquefaction, steel alloy processing, and military and defense equipment applications [2].

The latest report by the International Institute of Refrigeration states that the refrigeration and air conditioning sector accounts for 20 % of global energy demand [3]. Moreover, electricity consumption for space cooling is anticipated to increase threefold compared to present levels by the year 2050 [4]. This trend highlights the urgent need to improve the energy efficiency of refrigeration systems. In this regard, RSM offers an effective statistical tool for identifying optimal operating conditions with minimized computational or experimental efforts. This approach can significantly contribute to the design of more energy-efficient refrigeration systems.

Various studies have been conducted in the literature on two-stage cascade refrigeration systems. Ye et al. [5] conducted a study on the optimization of a two-stage cascade refrigeration system using response surface methodology. The predicted and actual values for COP and exergy efficiency showed maximum deviations of 0.84 % and 0.96 %. Ji et al. [6] conducted a comprehensive analysis of a two-stage cascade refrigeration system. Compared to the conventional R404A–R508B pair, the R290–R170 system improved COP by 5.94 % and reduced energy consumption by 5.68 %. Faruque et al. [7] examined the thermodynamic behavior of a two-stage cascade refrigeration system. T2BUTENE/toluene emerged as the most efficient pair, achieving a peak

* Corresponding author at: Department of Mechanical Engineering, University of Sakarya, TR-54050 Sakarya, Turkey.
E-mail address: safiyeozdemir@sakarya.edu.tr (S.N. Ozdemir).

https://doi.org/10.1016/j.applthermaleng.2025.129446
Received 22 July 2025; Received in revised form 21 November 2025; Accepted 8 December 2025
Available online 10 December 2025

Nomenclature

$\dot{E}_{dest}$	Total exergy destruction (kW)
$\dot{Q}_e$	Cooling load (kW)
P_{comp}	Total compressor power consumption (kW)
η_{elec}	Electrical efficiency (−)
η_{ex}	Exergy efficiency (−)
η_{mech}	Mechanical efficiency (−)
$\dot{Q}$	Heat transfer rate (kW)
a_0	Intercept
a_i	Linear coefficient
a_{ii}	Quadratic coefficient
a_{ij}	Interaction coefficient
$\dot{m}$	Mass flow rate (kg/s or g/s)
0	Reference state
Adeq	Adequate
Adj	Adjusted
ANN	Artificial Neural Network
ANOVA	Analysis of variance
ASHRAE	American Society of Heating, Refrigerating and Air-Conditioning Engineers
BBD	Box-Behnken design
CCD	Central composite design
CFC	Chlorofluorocarbon
CHX	Cascade heat exchanger
COP	Coefficient of performance
CRS	Cascade refrigeration system
D	Composite desirability function
d	Desirability index
EES	Engineering equation solver
GWP	Global warming potential
h	Specific enthalpy (kJ/kg)
HCFC	Hydrochlorofluorocarbon
HFC	Hydrofluorocarbon
HTC	High-temperature cycl
LTC	Low-temperature cycle
MAE	Mean Absolute Error
MTC	Medium-temperature cycle
NBP	Normal boiling point
ODP	Ozone depletion potential
Pred	Predicted
Prob	Probability
r	Relative importance
R	Response variable
R^2	Coefficient of regression
RMSE	Root Mean Squared Error
RSM	Response surface methodology
s	Specific entropy (kJ/kgK)
SS	Sum of squares
SSR	Regression sum of squares
SST	Total sum of squares
T	Temperature (°C)
x	Input variable
ΔT	Temperature difference (°C)
ε	Experimental error

Subscripts

c	condenser
comp	compressor
dest	destruction
e	evaporator
e	exit
ex	exergy
i	inlet

Table 1
Thermophysical characteristics of the refrigerants employed in the analyses [16].

Cycle	Refrigerant	ODP	$GWP_{100\text{-}yr}$ (CO_2-eq)	ASHRAE safety group	NBP (°C)	Molecular weight (kg mol^{-1})	Critical temperature (°C)	Critical pressure (MPa)
LTC	R1150	0	4	A3	−103.77	28.05	9.2	5.04
MTC	R170	0	5.5	A3	−88.58	30.07	32.17	4.87
HTC	R717	0	0	B2L	−33.33	17.03	132.25	11.33

COP of 1.957, minimum total compressor consumption of 6.2668 kW, and the highest exergy efficiency of 55.701 %. Ye et al. [8] conducted a thermodynamic investigation of an ultra-low temperature cascade refrigeration system using an ANN approach. The mean absolute errors in the predictions were 0.0027 for COP, 0.9090 for compressor power, 1.0314 for exergy destruction, and 0.1691 for exergy efficiency. Sun et al. [9] conducted a thermodynamic analysis of cascade refrigeration systems to assess various refrigerant combinations. The COP values for R41/R161 and R170/R161 ranged from 0.66 to 2.10 and 0.70 to 2.06, respectively, as evaporator temperature varied between −85 °C and −30 °C. Ustaoglu et al. [10] performed a comprehensive investigation of a vapor compression cascade refrigeration cycle. The highest achieved COP was 3.274, with an exergy efficiency of 37.63 % under optimal conditions. Roy and Mandal [11] carried out a numerical assessment of a cascade refrigeration system using two refrigerant pairs. Results revealed that the R170–R161 pair required less compressor input and provided a COP improvement of 6.7–8.9 % over the R41–R404A pair across the tested evaporator temperature range.

Research on three-stage cascade refrigeration systems has emerged too in recent years. Kayes et al. [12] tested ANN, XGBoost, and AdaBoost models in a triple-stage cascade refrigeration system, with ANN outperforming the others, yielding an R^2 of 1, RMSE of 143, and MAE of 76. Pektezel [13] performed the thermal design of a three-stage cascade refrigeration system. Among refrigerant combinations analyzed, R1150/R170/R717 provided the best performance, achieving a COP of 0.65 and an exergy efficiency of 0.35 at −85 °C. Walid Faruque et al. [2] conducted a thermodynamic evaluation of a triple-stage vapor compression cascade system. Findings revealed that the highest COP and exergy efficiency were 0.5931 and 54.446 %, respectively, at −100 °C. Hamzaoui et al. [14] conducted a study on a triple-stage cascade refrigeration system Results indicated that the system's COP is negatively related to the condensation temperature and positively related to the evaporation temperature, with COP varying between 0.35 and 0.9. Kayes et al. [3] performed an analysis of a 10 kW triple-stage cascade refrigeration system employing 1-butene/Heptane/m-Xylene as working fluids. Results indicated that as the evaporator temperature rose from −140 °C to −104 °C, COP and exergy efficiency improved by 91.2 % and 83.7 %, respectively.

Studies in the literature have indicated that the R1150/R170/R717 refrigerant group provides superior COP compared to other refrigerant

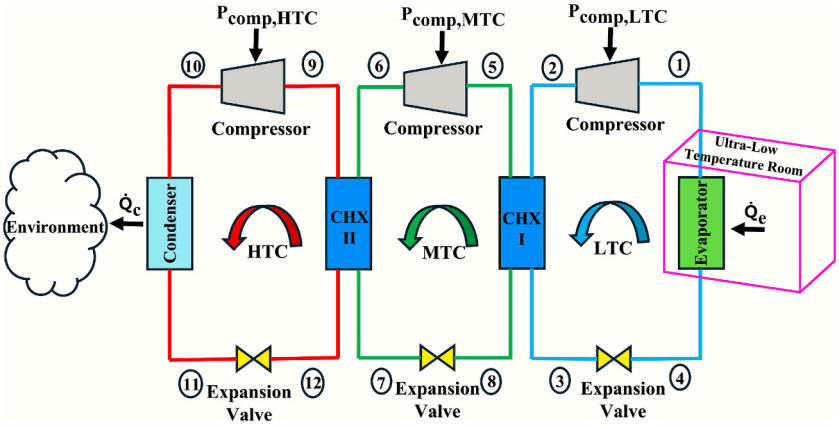

Fig. 1. Components and flow diagram of three-stage cascade refrigeration system.

Table 2
Thermodynamic formulations for each system equipment.

Equipment	Thermodynamic equations
Evaporator of LTC	$\dot{Q}_e = \dot{m}_{LTC}(h_1 - h_4)$ $\dot{E}_{dest,e} = \dot{E}_4 - \dot{E}_1 - \dot{E}_{Q,e}$ $\dot{E}_{Q,e} = \left(\frac{T_0}{T_L} - 1\right)\dot{Q}_e$
Compressor of LTC	$P_{comp,LTC} = \frac{\dot{m}_{LTC}(h_2 - h_1)}{\eta_m \eta_e}$ $\eta_{comp,LTC} = 0.874 - 0.0135\left(\frac{P_2}{P_1}\right) = \frac{h_{2s} - h_1}{h_2 - h_1}$ $\dot{E}_{dest,comp,LTC} = \dot{E}_1 - \dot{E}_2 + P_{comp,LTC}$
CHX-I	$\dot{m}_{LTC}(h_2 - h_3) = \dot{m}_{MTC}(h_5 - h_8)$ $\dot{E}_{dest,CHX,I} = \dot{E}_2 + \dot{E}_8 - \dot{E}_3 - \dot{E}_5$
Expansion valve of LTC	$h_3 = h_4$ $\dot{E}_{dest,valve,LTC} = \dot{E}_3 - \dot{E}_4$
Compressor of MTC	$P_{comp,MTC} = \frac{\dot{m}_{MTC}(h_6 - h_5)}{\eta_m \eta_e}$ $\eta_{comp,MTC} = 0.874 - 0.0135\left(\frac{P_6}{P_5}\right) = \frac{h_{6s} - h_5}{h_6 - h_5}$ $\dot{E}_{dest,comp,MTC} = \dot{E}_5 - \dot{E}_6 + P_{comp,MTC}$
CHX-II	$\dot{m}_{MTC}(h_6 - h_7) = \dot{m}_{HTC}(h_9 - h_{12})$ $\dot{E}_{dest,CHX,II} = \dot{E}_6 + \dot{E}_{12} - \dot{E}_7 - \dot{E}_9$
Expansion valve of MTC	$h_7 = h_8$ $\dot{E}_{dest,valve,MTC} = \dot{E}_7 - \dot{E}_8$
Compressor of HTC	$P_{comp,HTC} = \frac{\dot{m}_{HTC}(h_{10} - h_9)}{\eta_m \eta_e}$ $\eta_{comp,HTC} = 0.874 - 0.0135\left(\frac{P_{10}}{P_9}\right) = \frac{h_{10s} - h_9}{h_{10} - h_9}$ $\dot{E}_{dest,comp,HTC} = \dot{E}_9 - \dot{E}_{10} + P_{comp,HTC}$
Condenser of HTC	$\dot{Q}_c = \dot{m}_{HTC}(h_{10} - h_{11})$ $\dot{E}_{dest,c} = \dot{E}_{10} - \dot{E}_{11} - \dot{E}_{Q,c}$ $\dot{E}_{Q,c} = \left(1 - \frac{T_0}{T_H}\right)\dot{Q}_c$
Expansion valve of HTC	$h_{11} = h_{12}$ $\dot{E}_{dest,valve,HTC} = \dot{E}_{11} - \dot{E}_{12}$

Table 3
Design variables of thermodynamic model.

Parameter	Input value
$\dot{Q}_e$	10 kW
$\Delta T_{CHX,I}$	5 °C
$\Delta T_{CHX,II}$	5 °C
T_e	−120 °C, −105 °C, −90 °C
$T_{c,LTC}$	−70 °C, −55 °C, −40 °C
$T_{c,MTC}$	−30 °C, −15 °C, 0 °C
$T_{c,HTC}$	25 °C, 35 °C, 45 °C
η_{mech}	0.9
η_{elec}	0.95

Table 4
Characteristics of the reference model [18].

Parameter	Value/formulation
$\dot{Q}_e$	10 kW
T_e	−120 to −90 °C
$T_{c,LTC}$	Optimum value depending on T_e
$T_{c,MTC}$	Optimum value depending on T_e
$T_{c,HTC}$	40 °C
$\Delta T_{CHX,I}$ and $\Delta T_{CHX,II}$	5 °C
η_{comp}	0.874 − 0.0135 • Pressure Ratio
P_{comp}	$\dot{m}$ • Δh_{comp}
Superheating Degree at Compressor Inlets	12 °C at LTC and MTC, 5 °C at HTC
Refrigerant Type	R1150/R170/R161

combinations in three-stage cascade refrigeration systems [13–15]. Specifically, the refrigerant combination R1150/R170/R717 was chosen because previous studies reported its superior thermodynamic performance compared to other refrigerant groups. This superiority is not limited to COP but also extends to parameters directly related to the present study, such as exergy efficiency, compressor work, and exergy destruction. For example, the low normal boiling points of R1150 and R170 enable efficient operation at ultra-low temperatures, while the favorable thermophysical properties of R717 at the high stage contribute to reduced compressor power consumption and lower exergy destruction. The properties of the selected refrigerants are presented in Table 1.

In recent years, research on the optimization of thermal systems using RSM has gained momentum; nevertheless, studies applying RSM to the optimization of refrigeration systems remain quite limited. One of the motivations of this study is to derive quadratic equations that define the performance parameters of a three-stage cascade refrigeration system using RSM approach. In this way, researchers will be provided with the opportunity to test their own models using these equations. Another motivation of the study is to determine the optimum operating conditions using RSM, while reducing the number of experiments and associated costs. Determination of optimum operating parameters through RSM is expected to serve as a guide for future experimental investigations of three-stage cascade refrigeration systems. The findings obtained using RSM in this study are of particular importance for the optimal design of refrigeration systems intended to operate at ultra-low temperatures. Accordingly, the contribution of this study is methodological rather than configurational; the motivation is not to introduce a new three-stage cascade design—which is already a well-established refrigeration architecture—but to provide a comprehensive optimization framework for this conventional system through the application of RSM.

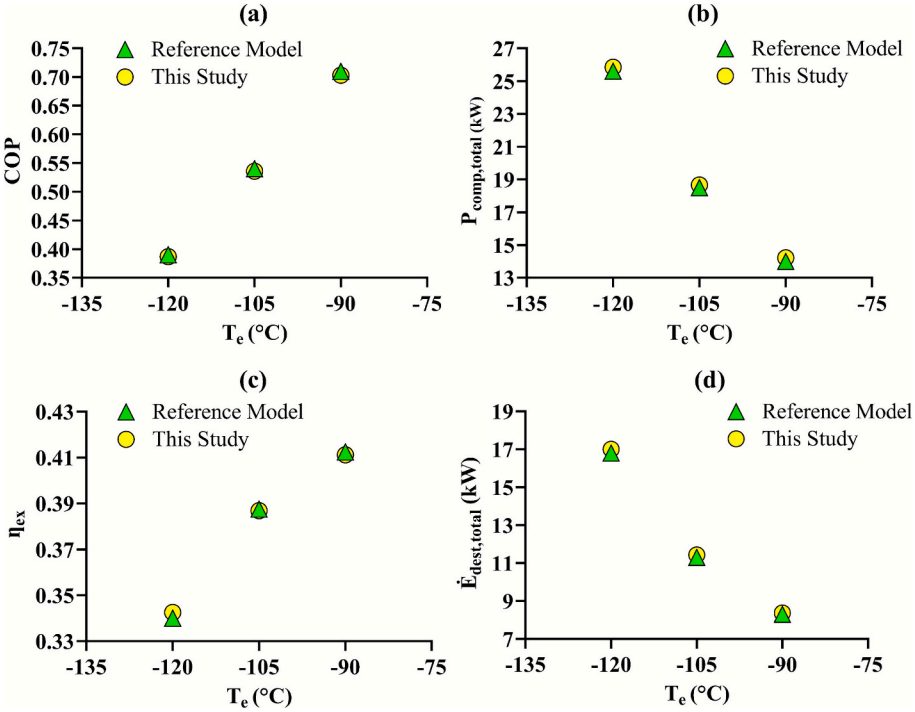

Fig. 2. Validation of the model.

Table 5
Experimental validation from the reference study [20].

Refrigerant	Parameter	Value	COP comparison
	Evaporator temperature	−10.23 °C	
	Condenser temperature	24.66 °C	Reference experimental
R134A	Mass flow rate	13.09 kg/h	study
			2.08
	Compressor power consumption	297.88 W	This study's EES model
	Superheating degree	11.09 °C	2.11
	Subcooling degree	3.85 °C	
	Evaporator temperature	−9.82 °C	
	Condenser temperature	25.24 °C	Reference experimental
R152a	Mass flow rate	8.06 kg/h	study
			2.17
	Compressor power consumption	278.55 W	This study's EES model
	Superheating degree	11.48 °C	2.19
	Subcooling degree	2.70 °C	
	Evaporator temperature	−9.71 °C	
	Condenser temperature	24.98 °C	Reference experimental
R1234yf	Mass flow rate	15.37 kg/h	study
			1.87
	Compressor power consumption	317.50 W	This study's EES model
	Superheating degree	9.28 °C	1.89
	Subcooling degree	6.37 °C	
	Evaporator temperature	−9.69 °C	
	Condenser temperature	25.06 °C	Reference experimental
R290	Mass flow rate	11.89 kg/h	study
			2.55
	Compressor power consumption	407.61 W	This study's EES model
	Superheating degree	5.63 °C	2.55
	Subcooling degree	2.56 °C	

2. Three-stage cascade refrigeration system

Fig. 1 illustrates the schematic representation of the three-stage cascade refrigeration system. Ultra-low temperature is attained using the refrigerant in the evaporator of the LTC. The compressor associated

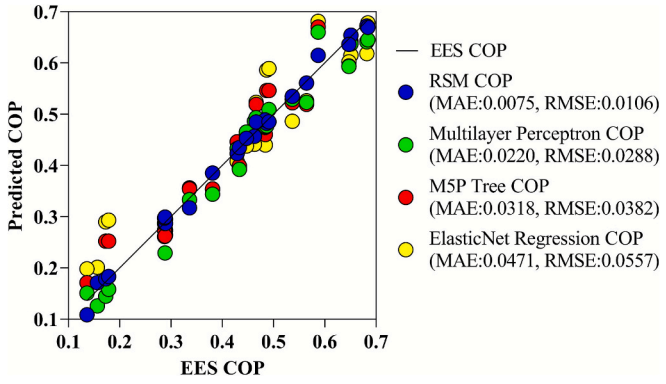

Fig. 3. Comparison of RSM with various artificial intelligence methods.

with the LTC elevates both the pressure and temperature of the refrigerant and directs it to the CHX—I. In this arrangement, CHX-I functions simultaneously as the condenser for the LTC and the evaporator for MTC. Afterward, the refrigerant undergoes pressure and temperature drop via the expansion valve. Within the MTC, thermal energy is absorbed from the LTC condenser through CHX—I. The refrigerant is then compressed by the compressor operating between state points 5 and 6. CHX-II acts as the condenser for the MTC and as the evaporator for HTC. After passing through the expansion valve located between points 7 and 8, the refrigerant's pressure and temperature decrease. In the evaporator of the HTC, heat is absorbed from the condenser of the MTC, maintaining thermal equilibrium between the released and absorbed heat. Subsequently, the compressor positioned between points 9 and 10 raises the pressure and temperature of the working fluid. The cycle concludes with heat rejection to the ambient environment via the condenser located between points 10 and 11, followed by expansion that lowers both pressure and temperature of the refrigerant, thereby completing the thermodynamic loop.

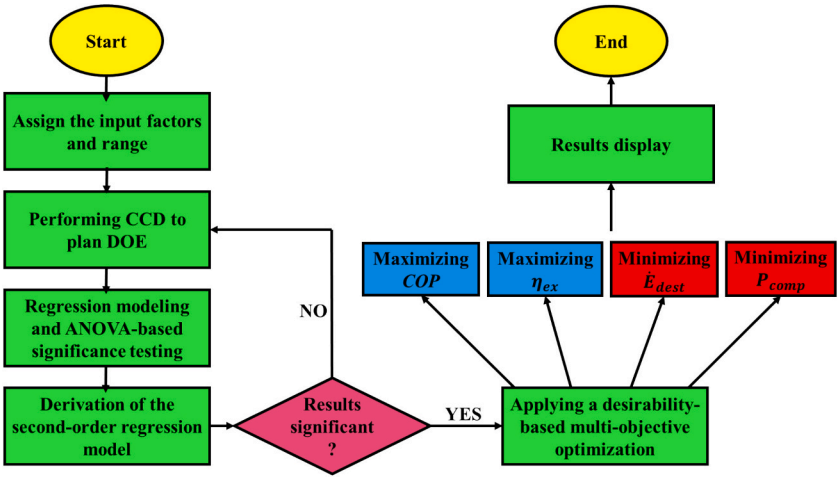

Fig. 4. Flow chart of RSM methodology.

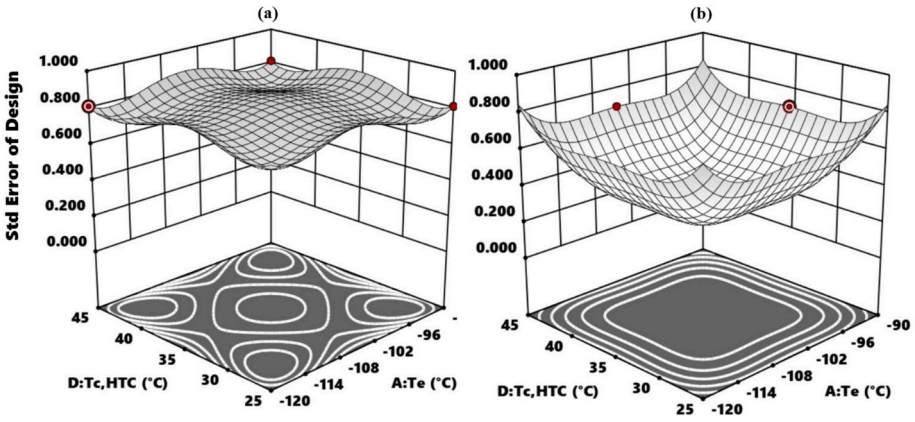

Fig. 5. 3D surface plot of standard error of CCD design for (a) jump to run of 15, (b) jump to run of 30.

2.1. Thermodynamic modeling of the system

The thermodynamic analysis of the system was conducted using the EES software [17]. The modeling process is based on the following assumptions:

1) All components are considered to operate under steady-state conditions.
2) Pressure drops, as well as heat losses or gains along the piping network, are assumed to be negligible.
3) Changes in kinetic and potential energy within system components are disregarded.
4) The electrical power consumption of fans associated with the condenser and evaporator is not taken into account.
5) Compression and expansion processes in compressors and expansion valves are considered adiabatic.
6) No subcooling is present at the outlet of the condensers; hence, the quality at state points 3, 7, and 11 is assumed to be zero.
7) No superheating occurs at the outlet of the evaporators; accordingly, the quality at state points 1, 5, and 9 is assumed to be unity. Although normal refrigeration systems have some superheat at the evaporator outlet, in this study the outlet is assumed to be a saturated vapor. This is a common modeling simplification and does not affect the optimization results, as the RSM focuses on the main performance trends rather than the small superheat at the evaporator outlet.
8) A temperature difference of 5 °C is assumed between the evaporator and the refrigerated room.
9) The condenser's heat sink temperature is assumed to be equal to the ambient temperature, which is taken as 25 °C with an atmospheric pressure of 101.325 kPa.
10) Air is assumed to be the external heat exchange medium interacting with the refrigerant in both the condenser and the evaporator.

COP of the system is defined with Eq. (1).

$$COP = \frac{\dot{Q}_e}{P_{comp,total}} \tag{1}$$

Total compressor consumption is calculated using Eq. (2).

$$P_{comp,total} = P_{comp,LTC} + P_{comp,MTC} + P_{comp,HTC} \tag{2}$$

Exergy of each state point is determined with Eq. (3).

$$e_i = (h_i - h_0) - T_0(s_i - s_0) \tag{3}$$

Flow exergy of state points in the system can be defined with multiplication of exergy and mass flow rate as given in Eq. (4).

$$\dot{E}_i = \dot{m}_i e_i \tag{4}$$

Total exergy destruction of the refrigeration system is calculated using Eq. (5).

Table 6
Design matrix with input factors and predicted responses.

Run	A:Te (°C)	B:Tc,LTC (°C)	C:Tc,MTC (°C)	D:Tc,HTC (°C)	R1:COP (−)	R2:η_{ex} (−)	R3:$\dot{E}_{dest}$ (kW)	R4:P_{comp} (kW)
1	−105	−40	−15	35	0.42327	0.298958	22.3601	29.5779
2	−105	−55	−15	35	0.484603	0.349686	12.8024	20.0221
3	−105	−55	−15	25	0.534803	0.383458	10.9363	18.1557
4	−120	−40	0	45	0.171052	0.145784	54.3111	63.1689
5	−105	−55	0	35	0.456725	0.329458	14.7696	21.989
6	−105	−55	−15	35	0.484603	0.349686	12.8024	20.0221
7	−90	−40	0	25	0.672186	0.39224	7.94105	13.7839
8	−120	−70	0	45	0.286845	0.25477	25.6414	34.4914
9	−120	−40	−30	25	0.178508	0.161134	48.7666	57.6222
10	−90	−70	0	25	0.614979	0.357376	14.1139	19.9514
11	−90	−40	0	45	0.560712	0.331726	11.3715	17.2208
12	−90	−70	−30	25	0.669586	0.393962	9.78217	15.6267
13	−105	−55	−15	35	0.484603	0.349686	12.8024	20.0221
14	−105	−55	−15	45	0.434992	0.31687	17.5689	24.7901
15	−120	−40	−30	45	0.108534	0.10522	61.115	69.9692
16	−105	−55	−15	35	0.484603	0.349686	12.8024	20.0221
17	−120	−70	−30	25	0.385201	0.33457	17.2775	26.1297
18	−105	−55	−30	35	0.45277	0.32747	16.0057	23.2268
19	−90	−70	−30	45	0.482212	0.278298	15.0026	20.8486
20	−105	−70	−15	35	0.488925	0.35987	8.44512	15.6579
21	−90	−40	−30	45	0.484869	0.282212	16.6767	22.5261
22	−120	−70	−30	45	0.297052	0.261907	27.1122	35.9617
23	−90	−70	0	45	0.48533	0.280112	15.0306	20.8733
24	−90	−40	−30	25	0.654068	0.381126	8.94254	14.7892
25	−120	−70	0	25	0.317269	0.289034	20.1105	28.9594
26	−105	−55	−15	35	0.484603	0.349686	12.8024	20.0221
27	−120	−55	−15	35	0.299036	0.255481	30.9393	39.7957
28	−120	−40	0	25	0.183301	0.163298	46.2664	55.1219
29	−105	−55	−15	35	0.484603	0.349686	12.8024	20.0221
30	−90	−55	−15	35	0.636058	0.378147	5.7219	11.5701

Table 7
ANOVA results.

Source	COP		η_{ex}		$\dot{E}_{dest}$		P_{comp}	
	SS	P-value Prob > F	SS	P-value Prob > F	SS	P-value Prob > F	SS	P-value Prob > F
Model	0.6643	<0.0001	0.1684	<0.0001	5921.39	<0.0001	6664.90	<0.0001
A:Te (°C)	0.5111	<0.0001	0.0677	<0.0001	2861.64	<0.0001	3585.07	<0.0001
B:Tc,LTC (°C)	0.0194	<0.0001	0.0167	<0.0001	871.32	<0.0001	871.95	<0.0001
C:Tc,MTC (°C)	0.0001	0.5857	0.0000	0.6555	6.88	0.4055	6.89	0.4046
D:Tc,HTC (°C)	0.0448	<0.0001	0.0200	<0.0001	197.96	0.0004	198.07	0.0003
AB	0.0365	<0.0001	0.0258	<0.0001	1045.15	<0.0001	1045.23	<0.0001
AC	0.0002	0.3903	0.0001	0.3495	2.25	0.6317	2.24	0.6324
AD	0.0098	<0.0001	0.0018	0.0003	21.29	0.1528	21.25	0.1529
BC	0.0053	0.0002	0.0023	0.0001	28.44	0.1021	28.41	0.1021
BD	0.0003	0.2463	0.0003	0.0908	6.32	0.4247	6.33	0.4242
CD	0.0033	0.0016	0.0015	0.0009	18.52	0.1804	18.49	0.1805
A^2	0.0008	0.0884	0.0028	<0.0001	79.18	0.0109	83.02	0.0094
B^2	0.0021	0.0082	0.0011	0.0031	17.52	0.1920	17.46	0.1924
C^2	0.0023	0.0061	0.0012	0.0022	17.32	0.1944	17.32	0.1941
D^2	2.251E-07	0.9753	5.922E-07	0.9349	5.45	0.4578	5.45	0.4574
R^2	0.9949		0.9924		0.9768		0.9793	
Adj R^2	0.9901		0.9853		0.9551		0.9601	
Pred R^2	0.9589		0.9435		0.8909		0.9029	
Adeq Precision	52.9216		44.0576		25.5734		26.9771	

$$\dot{E}_{dest,total} = \dot{E}_{dest,e} + \dot{E}_{dest,comp,LTC} + \dot{E}_{dest,CHX,I} + \dot{E}_{dest,valve,LTC} + \dot{E}_{dest,comp,MTC} + \dot{E}_{dest,CHX,II} + \dot{E}_{dest,valve,MTC} + \dot{E}_{dest,comp,HTC} + \dot{E}_{dest,c} + \dot{E}_{dest,valve,HTC} \quad (5)$$

Exergy efficiency of three-stage cascade refrigeration configuration is determined using Eq. (6).

$$\eta_{ex} = 1 - \left(\frac{\dot{E}_{dest,total}}{P_{comp,total}}\right) \quad (6)$$

The energy and exergy balance equations corresponding to each system component are presented in Table 2.

The design specifications and input data used in the analysis are summarized in Table 3. The evaporation temperatures (−120, −105, −90 °C) represent ultra-low temperature operation zones commonly required in cryogenic cooling, biomedical preservation, and special freezing applications. The condensation temperatures of the LTC (−70, −55, −40 °C) allow realistic modeling of the LTC rejecting heat to the MTC under different operating scenarios. The condensation temperatures of the MTC (−30, −15, 0 °C) ensure that the temperature differences across the cascade heat exchangers remain thermodynamically reasonable, thus reflecting practical cascade operation. The condensation temperatures of the HTC (25, 35, 45 °C) correspond to ambient conditions encountered in different climates.

In practical operations, compressor efficiency is influenced by factors such as the type of refrigerant, compression ratio, and temperature range. Since different working fluids are used at each stage, applying the

Table 8
Regression coefficient table.

Responses	R1	R2	R3	R4
Intercept	2.290890	0.152179	78.275100	81.368500
A	0.013009	−0.014120	2.637610	2.660660
B	0.006331	0.006613	−2.272150	−2.274320
C	−0.001217	−0.001044	0.403481	0.403040
D	−0.019452	−0.008694	−1.368200	−1.367540
AB	0.000212	0.000178	−0.035921	−0.035922
AC	0.000015	0.000010	0.001665	0.001661
AD	−0.000165	−0.000072	−0.007690	−0.007683
BC	0.000081	0.000053	−0.005926	−0.005922
BD	0.000030	0.000028	0.004190	0.004192
CD	0.000096	0.000064	−0.007173	−0.007167
A^2	−0.000076	−0.000146	0.024570	0.025159
B^2	−0.000127	−0.000090	0.011557	0.011537
C^2	−0.000133	−0.000094	0.011490	0.011492
D^2	0.000003	0.000005	0.014502	0.014508

same isentropic efficiency correlation may not accurately reflect the performance characteristics of individual compressors. For this reason, the optimization outcomes may deviate from actual operating conditions. On the other hand, in this theoretical study, the pressure ratio term at the end of the isentropic efficiency formula produces different values for each stage and gas. The pressure ratio is defined as P2/P1 for LTC, P6/P5 for MTC, and P10/P9 for HTC. Therefore, isentropic efficiency varies depending on the gas and the stage considered. As a result, the chosen method offers a robust and computationally efficient framework for the real operation and optimization of multi-stage cascade refrigeration systems.

2.2. Model validation

The design parameters of the three-stage cascade refrigeration cycle, as provided in Table 4 and originally proposed by Sun et al. [18], were implemented in the EES-based model developed in this study. As shown in Fig. 2a, for evaporation temperatures of −120, −105, and − 90 °C, the deviations between the two models remain below 1 % (0.8 %, 0.76 %, and 0.95 %, respectively), confirming the high consistency and reliability of the developed model. As depicted in Fig. 2b, for evaporation temperatures of −120, −105, and − 90 °C, the differences are 0.98 %, 0.86 %, and 1.57 %, respectively, which demonstrates the accuracy and reliability of the proposed approach. As illustrated in Fig. 2c, at evaporation temperatures of −120, −105, and − 90 °C, the deviations are 0.74 %, 0.15 %, and 0.31 %, respectively, all remaining well below 1 %, which confirms the robustness of the developed model. As presented in Fig. 2d, for evaporation temperatures of −120, −105, and − 90 °C, the deviations are 1.19 %, 1.24 %, and 0.88 %, respectively, all within a narrow margin, indicating the reliability and consistency of the developed model.

Since no experimental data for three-stage cascade refrigeration systems are available in the literature, a full experimental validation of the present model cannot be performed. Therefore, in addition to the theory-to-theory comparison, the fundamental thermodynamic behavior of the model was validated using experimental data from a well-documented single-stage vapor compression refrigeration cycle. This approach has also been adopted in earlier cascade refrigeration studies when experimental data for higher-stage configurations are unavailable [3,19]. In this context, the COP values reported in the

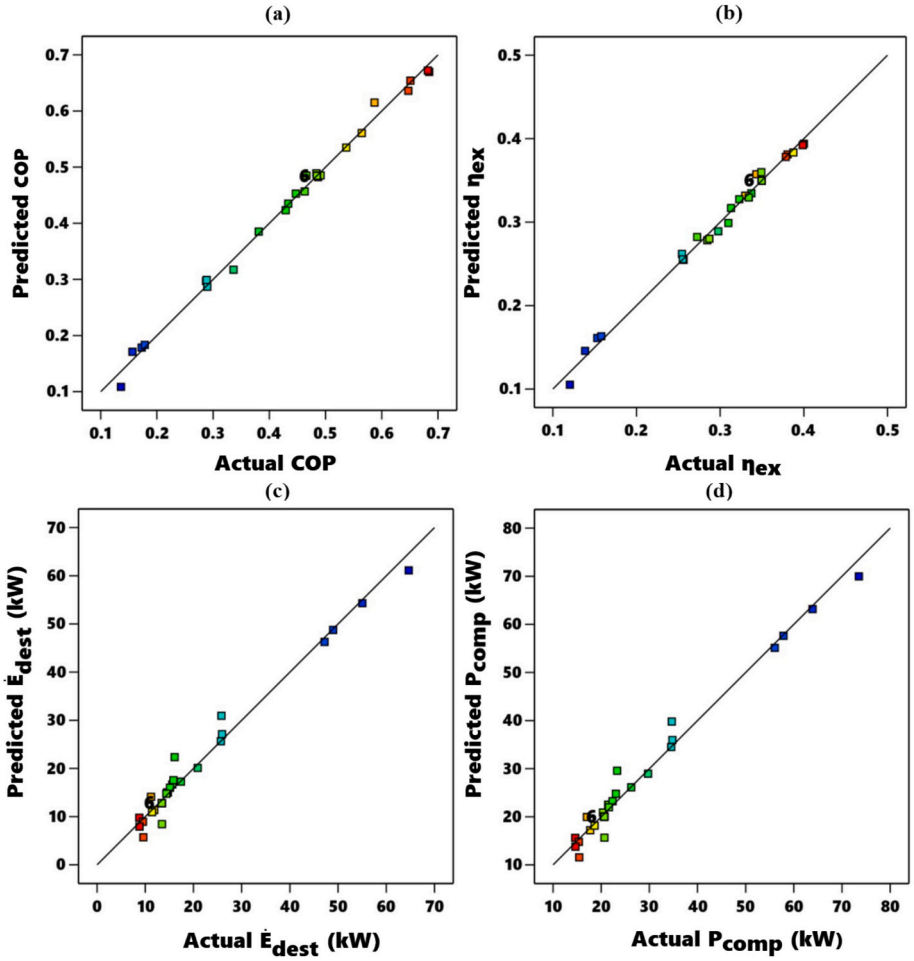

Fig. 6. Validation of regression model predictions compared to actual results.

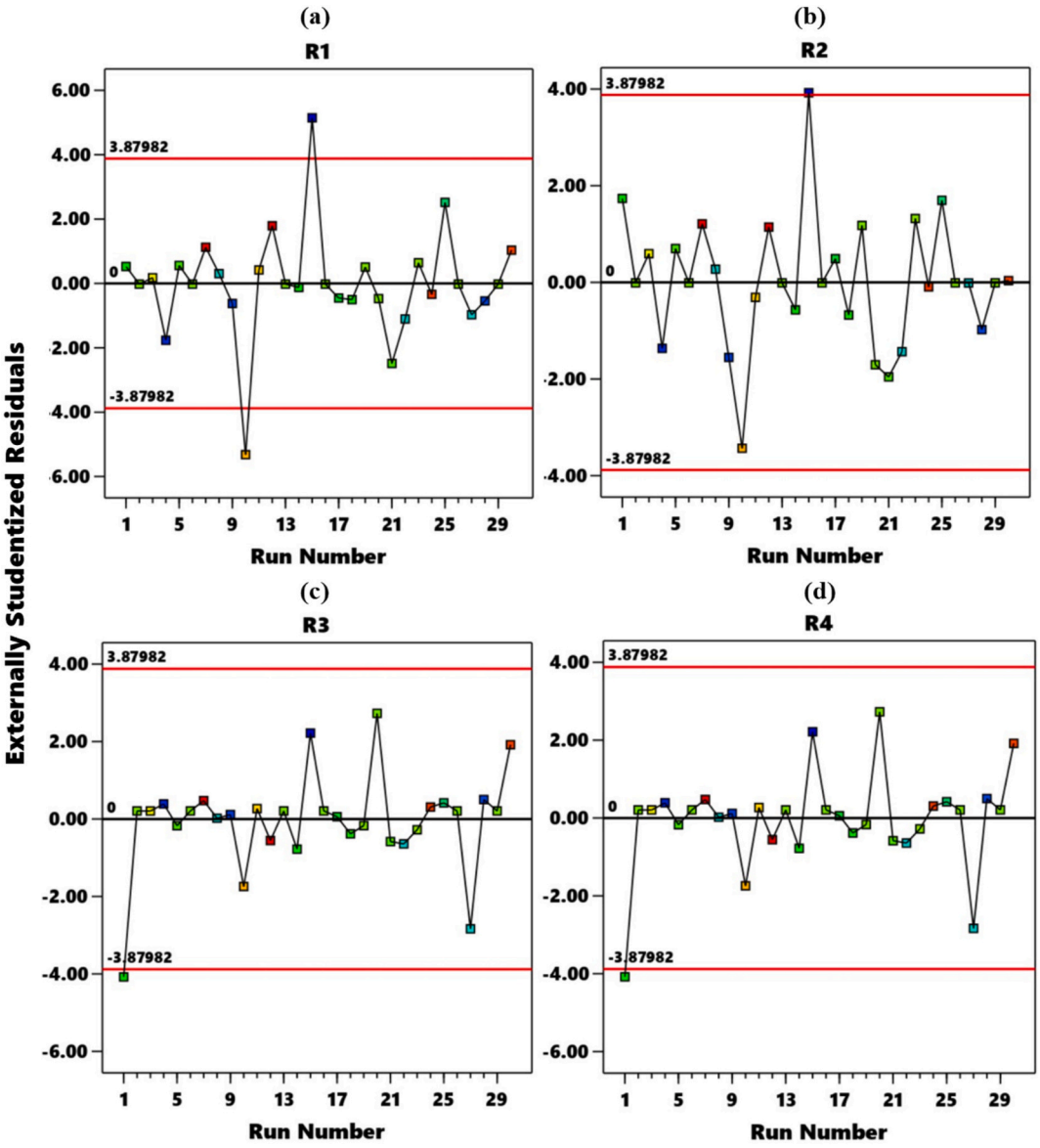

Fig. 7. Distribution of externally studentized residuals against run number for model accuracy diagnostics.

experimental single-stage vapor compression refrigeration study conducted by Sánchez et al. [20], as summarized in Table 5, were compared with the COP values calculated by the EES model used in the present work. The comparison, performed for four different refrigerants, shows a very close agreement between the experimental values and the model predictions. This result demonstrates that the thermodynamic behavior of a single-stage subsystem—forming the fundamental basis of the three-stage cascade cycle—is in strong accordance with experimentally validated data, thereby supporting the reliability of the overall model.

3. Motivation for selecting RSM in refrigeration system optimization

COP values obtained from the EES model created in this study were predicted using four different techniques: RSM, Multilayer Perceptron neural network, M5P decision tree, and ElasticNet regression to determine the most suitable method for optimizing a three-stage cascade refrigeration system. The results are presented in Fig. 3. In this figure, the proximity of the circles to the diagonal line indicates the accuracy and superiority of the corresponding method in predicting COP values. It is observed that the COP values predicted by RSM are distributed very closely along the diagonal line, whereas the other methods exhibit noticeable deviations. An R^2 of 0.9949 for RSM corresponds to explaining more than 99 % of the variance in COP values, leaving only ~0.5 % unexplained. In contrast, an R^2 of 0.9679 for MLP leaves more than 3 % unexplained variance. Although this difference may seem numerically small, it translates into noticeably higher prediction errors, as also reflected in the MAE and RMSE (0.0075 and 0.0106 for RSM vs. 0.0220 and 0.0288 for MLP).

Thermodynamic behavior of a three-stage cascade system is inherently nonlinear. RSM employs quadratic models that include both interaction terms (e.g., $T_e \times T_{c,LTC}$) and second-order (squared) terms (e.g., T_e^2, $T_{c,LTC}^2$), allowing it to explicitly capture nonlinear and synergistic effects between input variables. The interaction terms like $T_e \times T_{c,LTC}$ explicitly quantify the combined effect of evaporation and LTC condenser temperatures on COP. The second-order terms such as T_e^2 and $T_{c,LTC}^2$ capture nonlinear trends that a purely linear or purely data-driven regression might miss. Therefore, RSM not only minimizes prediction errors but also provides a transparent mathematical framework for understanding the system's response to input interactions, which is critical for cascade refrigeration optimization. In contrast, standard MLP, M5P, or ElasticNet models in the study rely on purely data-driven fitting,

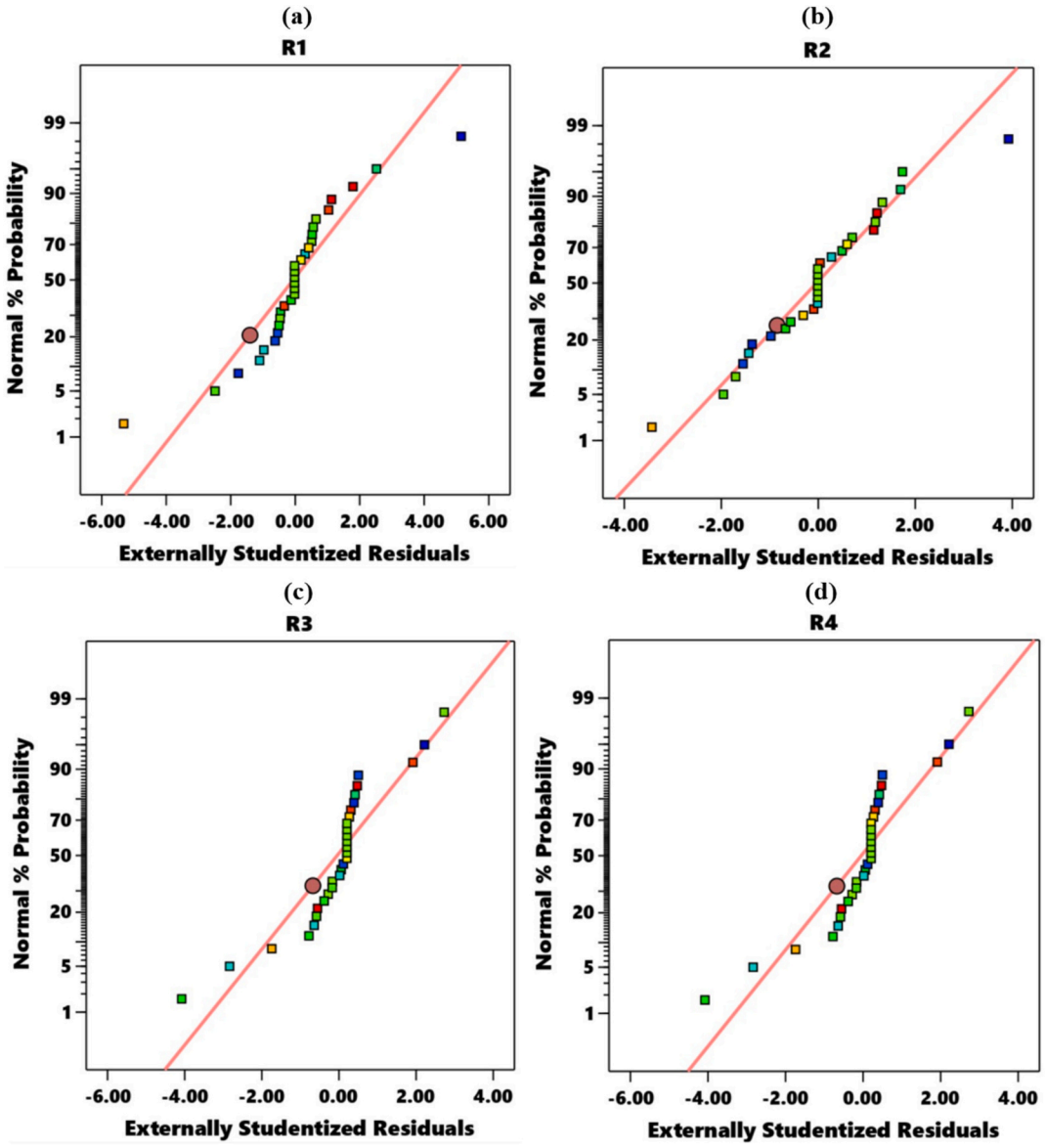

Fig. 8. Normal probability plots for RSM models.

which may approximate nonlinearities but do not explicitly represent the physical or synergistic interactions in the model.

4. Response surface methodology

RSM is a widely used Design of Experiments (DOE) approach that transforms linear factorial designs into quadratic models by incorporating axial and central points into these designs. This methodology effectively reduces the number of experimental runs, allowing for precise and reliable results at a lower cost and effort [21]. The flow chart in Fig. 4 outlines the systematic procedure of the RSM-based approach used for experimental design and optimization. A quadratic regression model, which incorporates linear, squared, and interaction effects of the input factors $x_1, x_2, \ldots, x_j$, can be represented by Eq. (7) [22].

$$R = a_0 + \sum_{i=1}^{j} a_i x_i + \sum_{i=1}^{j} a_{ii} x_i^2 + \sum_{i=1}^{j} \sum_{j=i+1}^{j} a_{ij} x_i x_j + \varepsilon \quad (7)$$

where R is the objective function; x_i and x_j show the input factors; a_0 is an intercept, and a_i, a_{ii}, and a_{ij} are the linear, quadratic, and interaction coefficients, and ε is the experimental error, respectively. In this study, the cascade refrigeration system comprises four input factors; thus, the RSM equation is formulated as follows [23]:

$$R = a_0 + a_1x_1 + a_2x_2 + a_3x_3 + a_4x_4 + a_{11}x_1^2 + a_{22}x_2^2 + a_{33}x_3^2 + a_{44}x_4^2 + a_{12}x_1x_2 + a_{13}x_1x_3 + a_{14}x_1x_4 + a_{23}x_2x_3 + a_{24}x_2x_4 + a_{34}x_3x_4 + \varepsilon \quad (8)$$

In this study, CCD was chosen for its advantages, such as effectively analyzing decision variables across a wide range, accurately estimating model curvature, and providing significant statistical power for lack-of-fit tests. A five-level CCD was developed using four independent variables to generate a second-order polynomial model. This design comprised 16 factorial (cubic) points, 8 axial points, and 6 center points, resulting in a total of 30 experimental runs.

As illustrated in Fig. 5(a), the standard error values exhibit a homogeneous distribution across the response surface, indicating that the model provides more reliable predictions of the response variable within the design space. In Fig. 5(b), the design space features a concave surface structure, with larger standard errors observed at its edges. However, the maximum standard error values range from 0.6 to 0.8, indicating that the model maintains acceptable sensitivity and predictive reliability within the design space [24]. The experimental design, detailed in

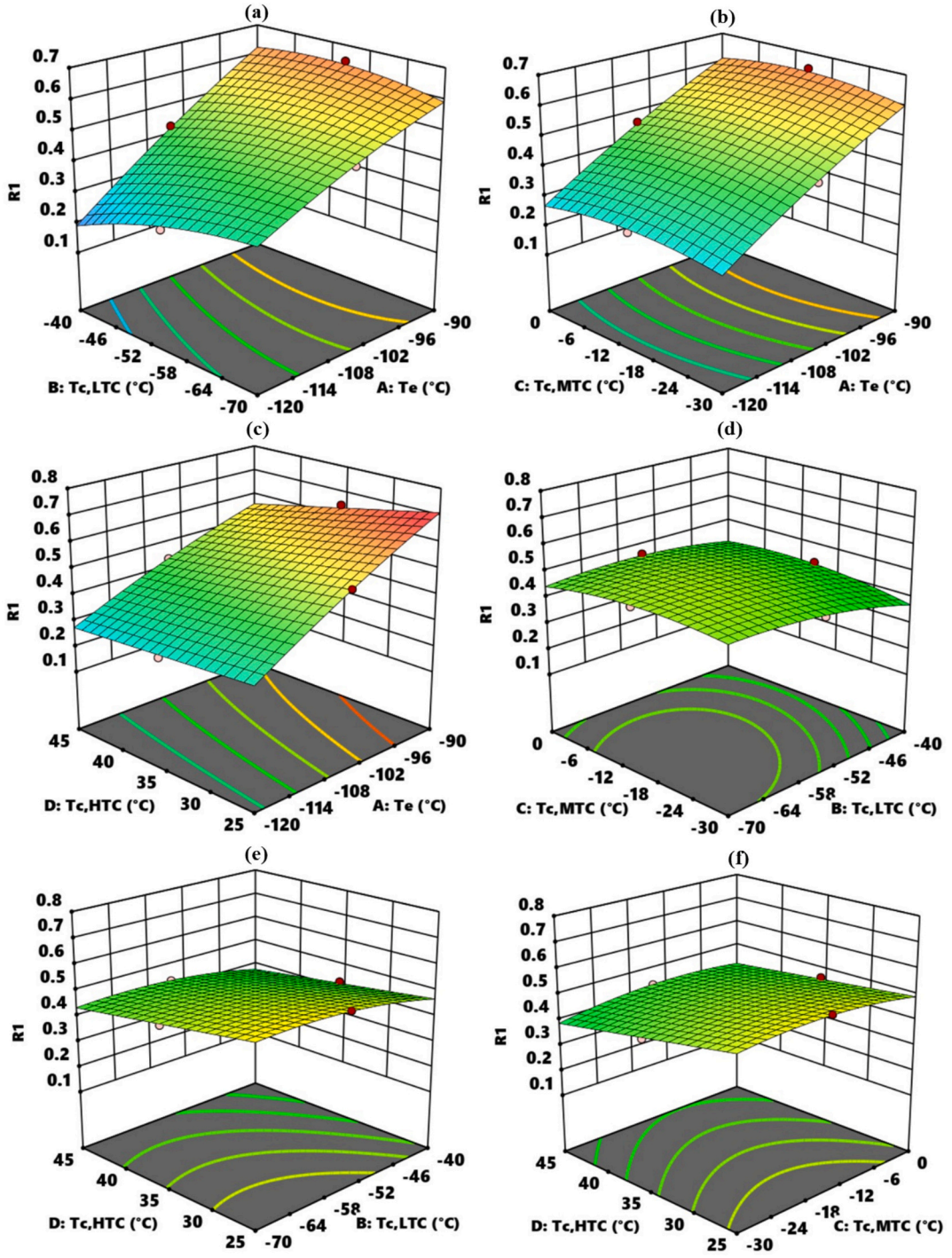

Fig. 9. 3D response surface plots showing the interaction effects of four input factors on COP.

Table 6, outlines the four chosen input parameters and their specified ranges and corresponding predicted values, following the DOE methodology.

Thermodynamic performance data, including the COP, exergy efficiency, total compressor power consumption, and exergy destruction, were initially calculated using EES. These results were then imported into Design-Expert 13 software (trial version, Stat-Ease Inc., Minneapolis, USA) to conduct a quadratic regression analysis based on RSM. The adequacy of the model was verified through ANOVA, and the Derringer desirability function was utilized for multi-objective optimization. This approach enabled the simultaneous improvement of COP and exergy efficiency while minimizing both compressor power consumption and exergy destruction.

5. Results and discussions

5.1. Analysis of variance

The ANOVA results are presented in Table 7. The regression coefficients were determined as 0.9949, 0.9924, 0.9768, and 0.9793 for COP, η_{ex}, $\dot{E}_{dest}$, and P_{comp}, respectively. Adj R^2 refines the regression coefficient by considering the number of predictors, penalizing non-significant terms. In contrast, Pred R^2 assesses the model's capacity to predict new, unseen data, typically using cross-validation [25]. The

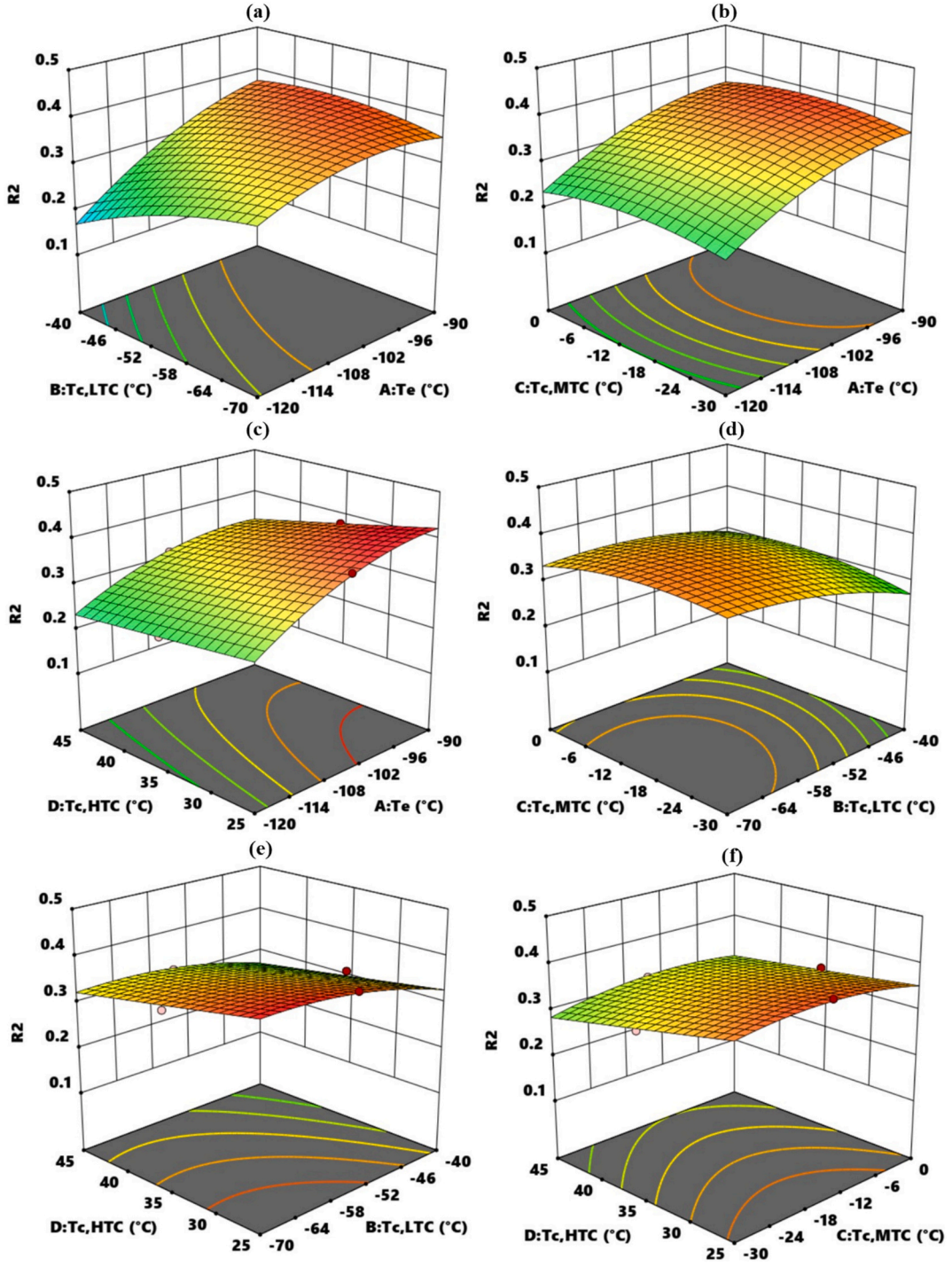

Fig. 10. 3D response surface plots showing the interaction effects of four input factors on exergy efficiency.

difference between Adj R^2 and Pred R^2 being less than 0.2 indicates that the regression models were developed with high compliance and reliability. From ANOVA results, the statistical significance of linear, interaction, and squared terms has been assessed using probability values at a 95 % confidence level ($p < 0.05$) [26]. Among the linear terms, input factors A (T_e), B ($T_{c,LTC}$), and D ($T_{c,HTC}$) were found to be statistically significant across all regression models. In contrast, factor C ($T_{c,MTC}$) was statistically insignificant in all cases, indicating a limited impact on system performance. The inclusion of $T_{c,MTC}$, despite its limited statistical significance, was crucial in capturing the interaction dynamics between cascade stages and thermodynamic constraints. This comprehensive representation mitigates the risk of biased model reduction, ensuring that the resulting optimization outcomes remain applicable to practical three-stage systems. The MTC operates as an intermediate bridge between LTC and HTC. As a result, variations in $T_{c,MTC}$ directly affect the inlet conditions of the HTC; however, their influence on overall system performance is limited. Regarding the interaction terms, the interaction between factors A and B (AB) consistently showed significance ($p < 0.0001$), suggesting a strong synergistic effect between the evaporator and low-temperature condenser temperatures. Other interaction terms (AC, AD, BC, BD, CD) had *p*-values greater than 0.05 in most models, indicating weak or negligible interactive influences. For the squared terms, A^2 and B^2 were significant in selected

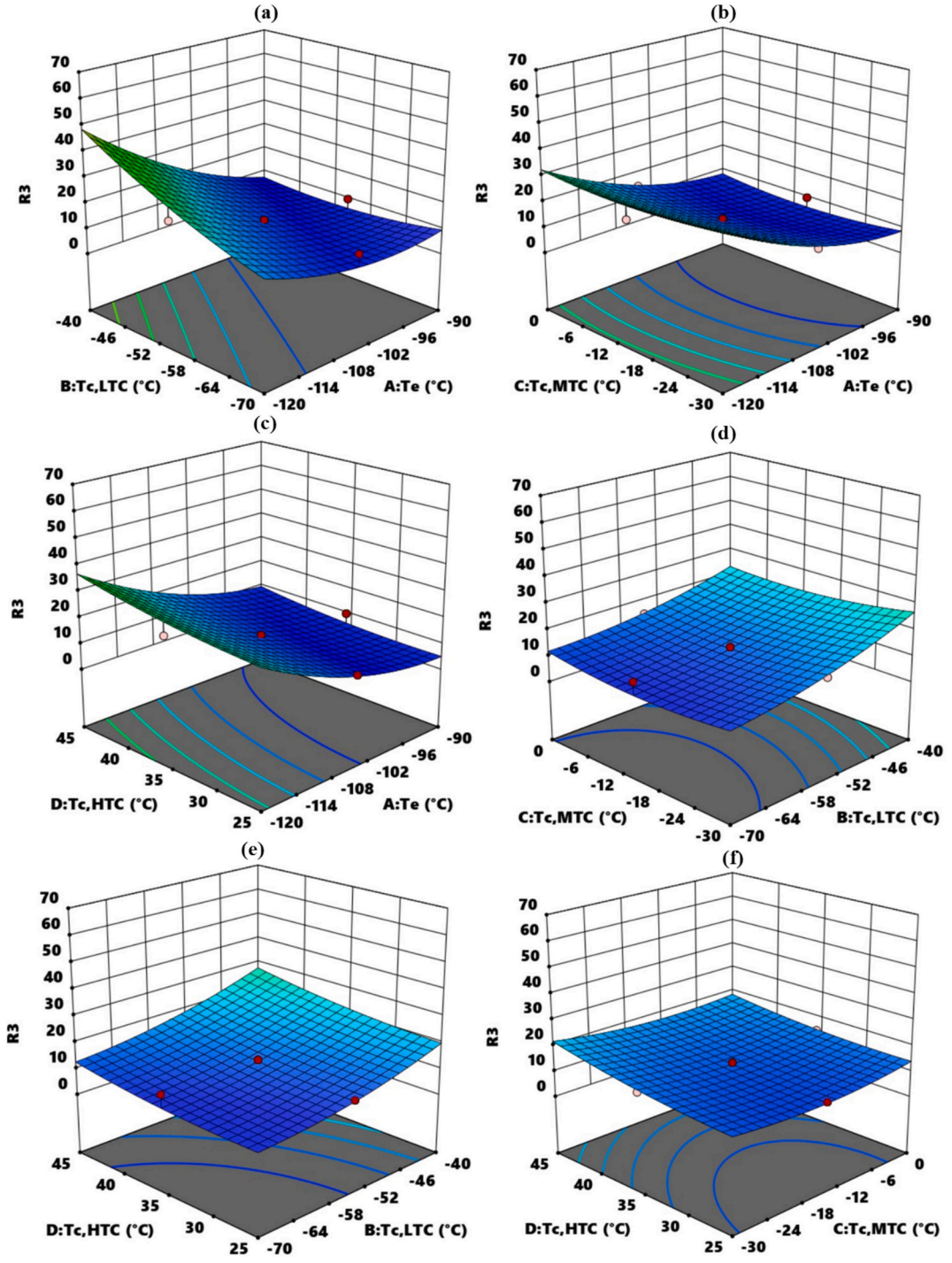

Fig. 11. 3D response surface plots showing the interaction effects of four input factors on total exergy destruction.

responses, particularly η_{ex} and $\dot{E}_{dest}$. Conversely, D^2 was consistently insignificant, suggesting that this factor predominantly has a linear effect. The signal-to-noise (S/N) ratio for each regression model is evaluated using the Adequate Precision (Adeq Precision) value. Among all the models assessed, the COP model demonstrated the highest sensitivity, achieving an Adeq Precision value of 52.9216. This indicates a highly reliable response. Furthermore, all other models also yielded Adeq Precision values exceeding the threshold of 4, confirming that each regression model maintains an acceptable S/N ratio and can be considered statistically valid and predictive [27].

5.2. Regression equations of responses

In this study, the impact of input factors on the four response parameters has been analyzed using a quadratic mathematical model derived from the CCD.

$$R = b_0 + b_1A + b_2B + b_3C + b_4D + b_5AB + b_6AC + b_7BC + b_8AD + b_9BD + b_{10}CD + b_{11}A^2 + b_{12}B^2 + b_{13}C^2 + b_{14}D^2 \quad (9)$$

where R is the reponse; b_0 is the intercept, $b_1, b_2, \ldots, b_{14}$ are regression coefficients. A, B, C, D are linear effects; AB, AC, BC, AD, BD, and CD are interaction effects; A^2, B^2, C^2, and D^2 are quadratic terms. Regression

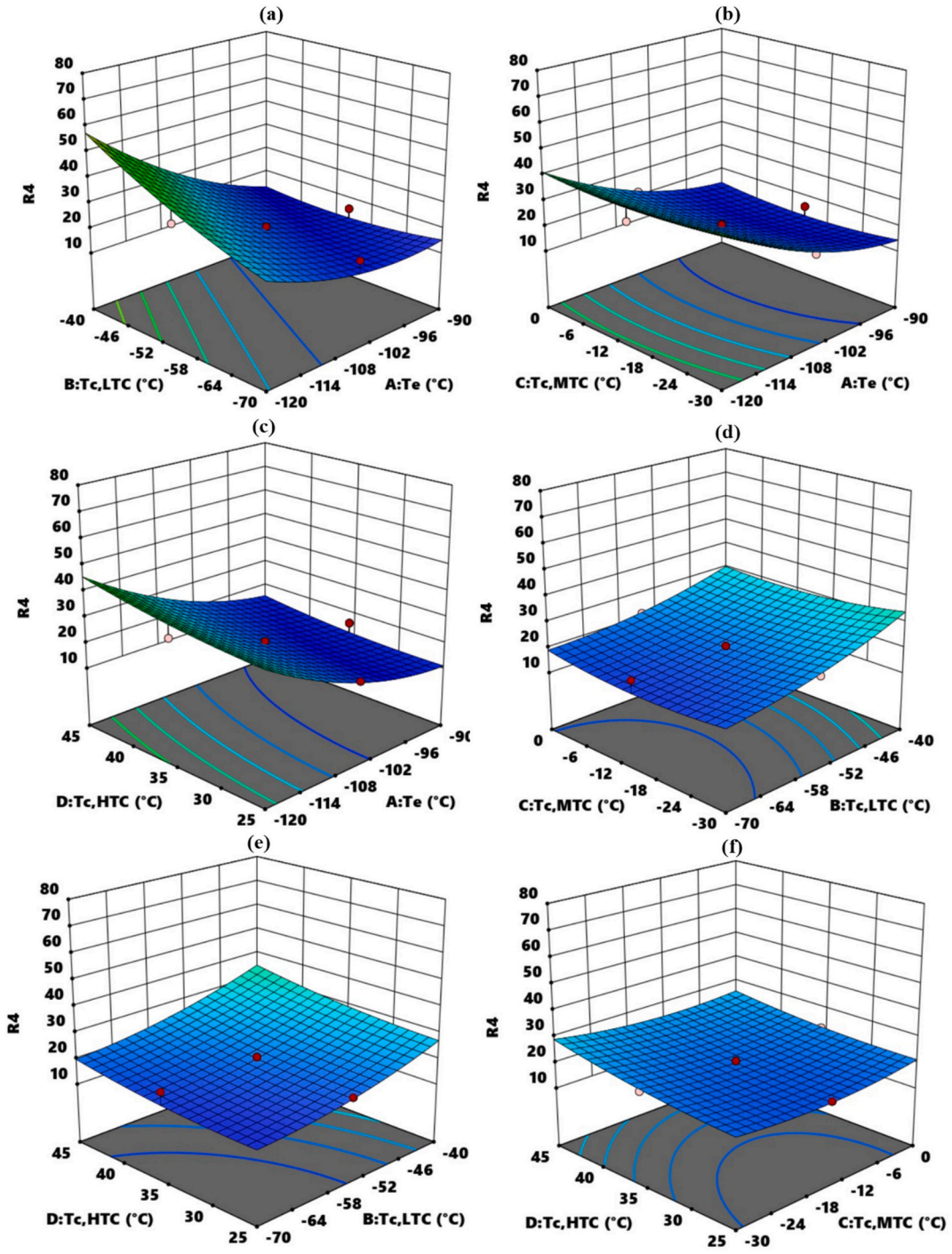

Fig. 12. 3D response surface plots showing the interaction effects of four input factors on compressor power consumption.

Table 9
Constraints.

Parameter	Target	Lower limit	Upper limit	Weight
A:Te (°C)	is in range	−120	−90	3
B:Tc,LTC (°C)	is in range	−70	−40	3
C:Tc,MTC (°C)	is in range	−30	0	3
D:Tc,HTC (°C)	is in range	25	45	3
R1:COP (−)	maximize	0.1361	0.6843	5
R2:η_{ex} (−)	maximize	0.1204	0.4001	5
R3:$\dot{E}_{dest}$ (kW)	minimize	8.766	64.65	5
R4:P_{comp} (kW)	minimize	14.61	73.5	5

coefficients for each response model were presented in Table 8. A positive coefficient indicates that an increase in the associated input factor increases the response variable. Conversely, a negative coefficient indicates that an increase in the input decreases the response.

Fig. 6 presents the comparison between predicted and actual results for all performance indicators. The distribution of actual data points along the reference line in all graphs shows that the regression models developed using RSM have a high regression coefficient and exhibit a strong correlation with the experimental data.

Residuals were plotted against experimental runs in Fig. 7 to identify any unexpected observations that could violate model assumptions. The horizontal red lines indicate the critical threshold value of the externally

Table 10
Optimized results.

Optimal combination				Predicted responses			
A (°C)	B (°C)	C (°C)	D (°C)	R1 (−)	R2 (−)	R3 (kW)	R4 (kW)
−90.043	−56.411	−10.941	26.077	0.697	0.414	5.545	11.394

Table 11
Effect of response weight levels on the optimal solution.

Optimal combination				Predicted responses			
Weight	A (°C)	B (°C)	C (°C)	D (°C)	R1 (−)	R2 (−)	R3 (kW)	R4 (kW)
1	−90.134	−50.075	−1.959	25.030	0.684	0.404	7.032	12.888
2	−91.040	−53.626	−18.958	26.663	0.688	0.414	4.963	10.897
3	−90.550	−44.032	−19.697	26.003	0.685	0.407	5.684	11.576
4	−90.820	−55.576	−12.586	27.040	0.685	0.412	5.190	11.105
5	−90.043	−56.411	−10.941	26.077	0.697	0.414	5.545	11.394

studentized residuals (±3.87982). Data points that exceed these lines are classified as outliers and may pose a danger to model validation. The analysis indicated that a significant portion of the residuals is under the critical threshold values, which supports the validity and statistical reliability of the model.

The normal probability plots used to assess the models display the standardized residuals for quadratic models (Figs. 8(a–d)). The normal probability plot of the residuals shows that they are normally distributed, as the data points are mostly aligned along the linear reference line. This alignment supports the validity and adequacy of the regression model based on the least squares method, indicating that the model is both suitable and reliable for predicting system performance.

5.3. Interactive effect analysis

Figs. 9(a–c) show the interactive effects of T_e and T_c on COP for $T_{c,LTC}$, $T_{c,MTC}$, and $T_{c,HTC}$, respectively. At a fixed evaporator temperature of −120 °C, lowering the $T_{c,LTC}$ significantly increases the COP within the selected interval. Lower condensation temperatures enable the compressor to operate with reduced pressure differentials, which decreases energy consumption and improves the COP of the system (Fig. 9a). It is observed that COP increases with a higher evaporator temperature, indicating that T_e is crucial for maximizing the system's efficiency. In previous studies in the literature on cascade refrigeration systems, it has also been reported that the COP increases with increasing evaporator temperature [28,29]. On the other hand, the influence of binary combinations of condensation temperatures at different stages on the COP appears to be more limited in Figs. 9(d–f).

Figs. 10(a–c) present that the exergy efficiency of the cascade refrigeration system significantly increases as the evaporator temperature rises. A review of previous studies in the literature reveals that, similar to the findings of the present study, an increase in evaporator temperature has a positive effect on the exergetic efficiency of the system [30,31]. This trend indicates that higher evaporator temperatures reduce entropy generation due to smaller temperature differences during heat transfer, thereby enhancing the system's second law efficiency. In contrast, the impact of the binary interactions between LTC, MTC, and HTC condensing temperatures on the exergy efficiency is quite minimal in Figs. 10(d–f), indicating that the temperature changes on the condensing side have a very low impact on the total recoverable work potential of the system.

Fig. 11 shows that increasing the evaporator temperature reduces total exergy destruction in a cascade refrigeration system. Studies in the literature on cascade refrigeration systems have also indicated that an increase in evaporator temperature reduces the exergy destruction of the system [32,33]. In addition, $\dot{E}_{dest}$ reaches its minimum value of 8.766 kW when T_e and $T_{c,MTC}$ are −90 °C and − 30 °C. Under the same operating conditions, COP was 68.4 %, while exergy efficiency was 40 %. As shown in Fig. 11, T_e has a greater impact than other input factors. Figs. 11(d–f) shows that the interactions among $T_{c,LTC}$, $T_{c,MTC}$, and $T_{c,HTC}$ have little impact on total exergy destruction.

It can be observed from Fig. 12 that there is an inverse relationship between evaporator temperature and compressor power consumption. Studies in the literature have demonstrated that an increase in evaporator temperature leads to a reduction in compressor power consumption [34,35]. When T_e is fixed at −90 °C, $T_{c,LTC}$ at −70 °C, and $T_{c,HTC}$ at 25 °C, reducing $T_{c,MTC}$ from 0 °C to −30 °C results in approximately a 14.2 % decrease in total compressor power consumption (Fig. 12d). As shown in Fig. 12e, lowering the $T_{c,HTC}$ from 45 °C to 25 °C while keeping the T_e at −90 °C, $T_{c,LTC}$ at −70 °C, and $T_{c,MTC}$ at 0 °C results in an approximately 16.36 % reduction in compressor power consumption. As shown in Fig. 12f, the combination of the highest $T_{c,HTC}$ (45 °C) and the lowest $T_{c,MTC}$ (−30 °C) results in the maximum total compressor power consumption.

Among the input variables, T_e was identified as the most dominant factor affecting all performance metrics. Increasing T_e from −120 °C to −90 °C enhanced COP from 0.18 to 0.67 (approximately 270 %) and exergy efficiency from 0.16 to 0.39 (about 150 %), while reducing total compressor power consumption from 55.1 kW to 13.8 kW and overall exergy destruction from 46.3 kW to 7.9 kW. Overall, these results confirm that T_e is the main driver of system performance, followed by $T_{c,LTC}$ and $T_{c,HTC}$, whereas $T_{c,MTC}$ contributes negligibly.

5.4. Multi-objective optimization

In this study, the desirability approach is employed for optimization analysis because of its speed, simplicity, and flexibility advantages. Each response parameter in the Design-Expert software was converted into a dimensionless desirability value that ranges from 0 to 1. A desirability value of 0 represents an unacceptable situation, while a value of 1 indicates the highest level of acceptability. The Derringer desirability function was utilized and mathematically expressed in Eq. (10) to achieve the optimization objective [36].

$$D = \left(d_1^{r_1} \times d_2^{r_2} \times \ldots \times d_n^{r_n}\right)^{\frac{1}{\sum r_i}} = \left(\prod_{i=1}^{n} d_i^{r_i}\right)^{\frac{1}{\sum r_i}} \quad (10)$$

where D is the composite desirability function, d_i denotes the individual desirability index of the i-th response, r_i is the individual relative importance of the i-th response, and n indicates the total number of response variables. When all the desirability indices (d_i) achieve their optimal level ($d_i = 1$), D will also reach a value of 1 [37]. Table 9 presents

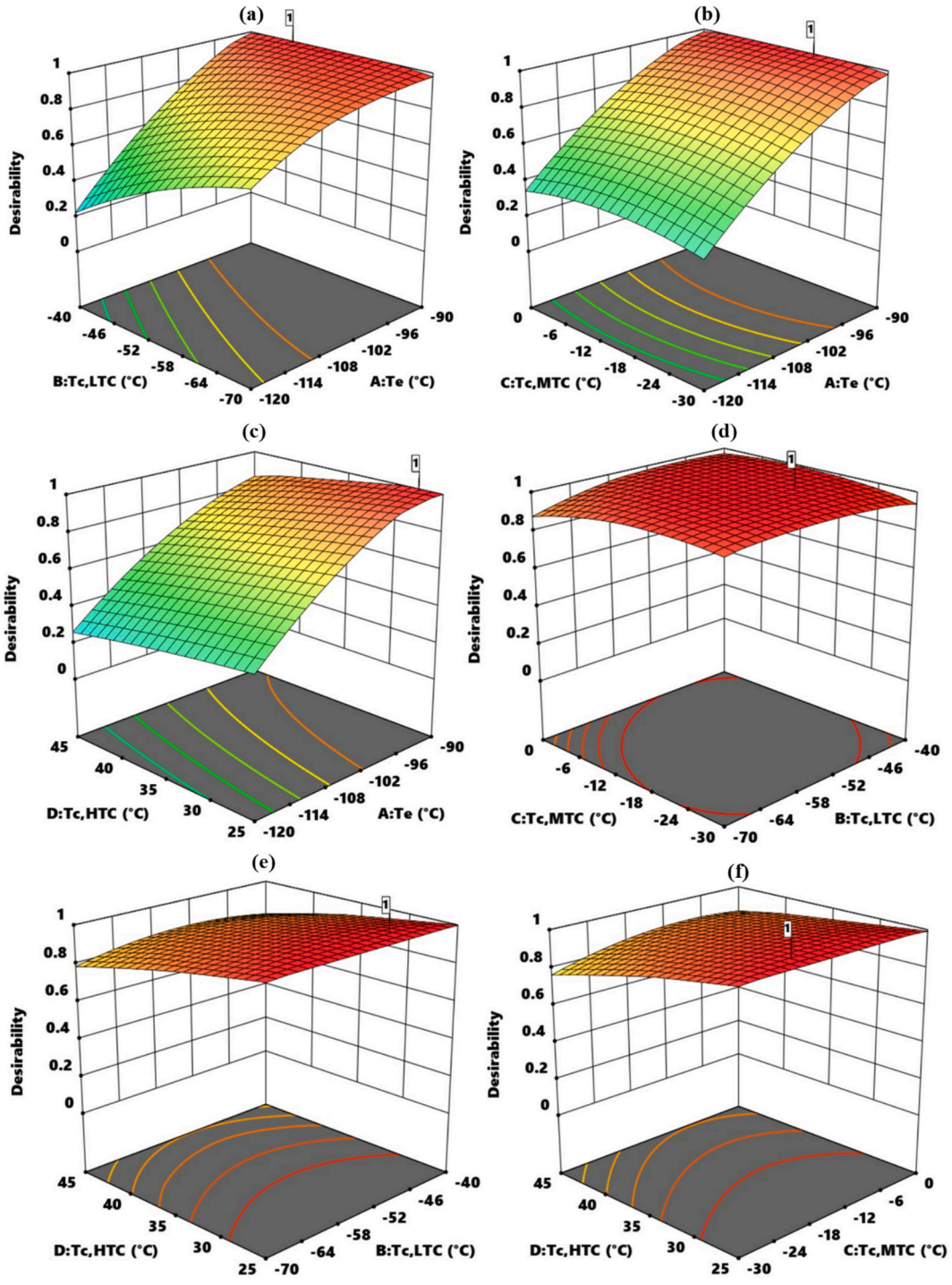

Fig. 13. 3D response surface plots on desirability.

the criteria for multi-objective desirability optimization. Thermal performance optimization results of the cascade refrigeration system based on the desirability approach are listed in Table 10. The optimal operating condition, corresponding to the highest overall desirability value, was obtained at an evaporator temperature of −90.043 °C, $T_{c,LTC}$ of −56.411 °C, $T_{c,MTC}$ of −10.941 °C, and $T_{c,HTC}$ of 26.077 °C. The optimal T_e represents a balance between achieving the required ultra-low cooling demand and limiting the thermodynamic irreversibilities associated with extremely low evaporation levels. The optimum $T_{C,LTC}$ provides an effective thermal match with the MTC evaporator, minimizing the temperature difference during interstage heat transfer and thereby reducing exergy destruction in the cascade heat exchanger. Similarly, the optimal $T_{C,MTC}$ improves thermal matching with the HTC evaporator by keeping the interstage temperature difference small. This reduces entropy generation in the second cascade heat exchanger and thereby lowers exergy destruction. Finally, the optimum $T_{C,HTC}$ represents a near-ambient rejection condition, which reduces the exergy loss during heat rejection to the environment. This optimum temperature configuration improves the thermodynamic matching between the cascade stages and thereby minimizes the overall exergy destruction in the system. In this study, all response weight values (R) were assigned a level of 5 because they represent key performance indicators of the CRS and

must be prioritized in the optimization process. The weight level of 3 displayed for input factors is a default software setting and does not affect the optimization process. To evaluate the robustness of the optimization, a weight sensitivity analysis (see Table 11) was conducted by varying the response weight between 1 and 5. The results showed that the evaporation temperature shifted only by about ±1–2 °C, while COP and exergy efficiency varied by less than 2–3 %. These findings confirm that the optimization process is robust to weight adjustments. All responses were given equal weight to avoid subjective prioritization and to establish a general optimization framework applicable to various ultra-low-temperature applications. Additionally, a weight-sensitivity analysis confirmed that the optimal conditions remain consistent, even when the relative importance of the responses is varied within a reasonable range.

Fig. 13 shows three-dimensional surface plots representing the overall desirability function concerning various pairs of input factors in the cascade refrigeration system. Specifically, the prevalence of red-colored areas near the surface peak in Fig. 13(d-f) highlights parameter combinations that yield high desirability, assisting in determining the best operating conditions.

6. Conclusions

In this study, the thermodynamic model of a three-stage cascade refrigeration system operating at ultra-low temperatures was developed using EES, and its performance was subsequently optimized through RSM. The input parameters included the evaporator temperature along with the condenser temperatures of all cycles, while the response parameters were defined as the COP, η_{ex}, $\dot{E}_{dest}$, and total compressor power consumption. Accurate and reliable second-order polynomial models were developed for four response parameters, and their validity was confirmed through ANOVA. The regression models created for the COP, η_{ex}, $\dot{E}_{dest}$, and P_{comp} showed a high level of agreement with the validated data. They achieved R^2 of 0.9949, 0.9924, 0.9768, and 0.9793, respectively. The multi-objective optimization aimed to maximize the COP and η_{ex} while minimizing $\dot{E}_{dest}$ and P_{comp}. The optimal operating conditions were determined as T_e of −90.043 °C, $T_{c,LTC}$ of −56.411 °C, $T_{c,MTC}$ of −10.941 °C, and $T_{c,HTC}$ of 26.077 °C. At these conditions, the system achieved a COP of 0.697, exergy efficiency of 41.4 %, total exergy destruction of 5.545 kW, and total compressor power consumption of 11.394 kW. These findings confirm that the combined EES–RSM framework provides a reliable, interpretable, and computationally efficient tool for optimizing the thermodynamic performance of multi-stage cascade refrigeration systems operating at ultra-low temperatures. The validity of the RSM-based quadratic model is limited to the specified design space, so caution is required when extrapolating beyond the tested operating region. While RSM allows for a clear understanding of the physical interactions among the decision variables, the model's predictions may be sensitive to small fluctuations in parameters. This sensitivity highlights the need for future uncertainty analyses and dynamic validation studies. Therefore, future work will focus on expanding the input factor ranges, incorporating experimental validation, and exploring adaptive optimization methods to enhance the model's generality and operational reliability.

CRediT authorship contribution statement

Oguzhan Pektezel: Writing – review & editing, Writing – original draft, Validation, Software, Resources, Methodology, Investigation. **Safiye Nur Ozdemir:** Writing – review & editing, Writing – original draft, Validation, Software, Resources, Methodology, Investigation.

Declaration of competing interest

The authors declare that they have no known competing financial interests or personal relationships that could have appeared to influence the work reported in this paper.

Data availability

The authors do not have permission to share data.

References

[1] M. Chen, Q. Yang, B. Shi, X. Chen, W. Chi, G. Liu, Y. Zhao, L. Li, Performance comparison of ultra-low temperature cascade refrigeration cycles using R717/R170, R717/R41 and R717/R1150 to replace R404A/R23, Thermal Sci. Eng. Progress 44 (2023).

[2] M. Walid Faruque, M. Hafiz Nabil, M. Raihan Uddin, M. Monjurul Ehsan, S. Salehin, Thermodynamic assessment of a triple cascade refrigeration system utilizing hydrocarbon refrigerants for ultra-low temperature applications, Energ. Conver. Manage: x 14 (2022).

[3] I. Kayes, R.E. Ratul, A. Abid, F.B. Majmader, Y. Khan, M.M. Ehsan, Multi-objective optimization and 4E (energy, exergy, economy, environmental impact) analysis of a triple cascade refrigeration system, Heliyon 10 (2024) e31655.

[4] Y. Dong, M. Coleman, S.A. Miller, Greenhouse gas emissions from air conditioning and refrigeration service expansion in developing countries, Annu. Rev. Environ. Resour. 46 (2021) 59–83.

[5] W. Ye, F. Liu, Y. Yan, Y. Liu, Application of response surface methodology and desirability approach to optimize the performance of an ultra-low temperature cascade refrigeration system, Appl. Therm. Eng. 239 (2024).

[6] S. Ji, Z. Liu, H. Pan, X. Li, Energy, exergy, environmental and exergoeconomic (4E) analysis of an ultra-low temperature cascade refrigeration system with environmental-friendly refrigerants, Appl. Therm. Eng. 248 (2024).

[7] M.W. Faruque, M.R. Uddin, S. Salehin, M.M. Ehsan, A comprehensive thermodynamic assessment of Cascade refrigeration system utilizing low GWP hydrocarbon refrigerants, Int. J. Thermofluids 15 (2022).

[8] W. Ye, Y. Yan, Z. Zhou, P. Yang, Parametric analysis and performance prediction of an ultra-low temperature cascade refrigeration freezer based on an artificial neural network, Case Stud. Therm. Eng. 55 (2024).

[9] Z. Sun, Q. Wang, Z. Xie, S. Liu, D. Su, Q. Cui, Energy and exergy analysis of low GWP refrigerants in cascade refrigeration system, Energy 170 (2019) 1170–1180.

[10] A. Ustaoglu, B. Kursuncu, M. Alptekin, M.S. Gok, Performance optimization and parametric evaluation of the cascade vapor compression refrigeration cycle using Taguchi and ANOVA methods, Appl. Therm. Eng. 180 (2020).

[11] R. Roy, B.K. Mandal, Energetic and exergetic performance comparison of cascade refrigeration system using R170-R161 and R41-R404A as refrigerant pairs, Heat Mass Transf. 55 (2018) 723–731.

[12] I. Kayes, M.H. Nabil, M.M. Ehsan, M.A. Habib, Y. Khan, Advanced exergy analysis and machine learning based multi-objective optimization of a modified triple cascade refrigeration system for enhanced performance, Appl. Therm. Eng. 274 (2025) 126661.

[13] O. Pektezel, Parametric analysis of a three-stage cascade refrigeration system for ultra-low temperature applications and performance prediction using multilayer perceptron algorithm, Sci. Technol. Built Environ. (2025) 1–25.

[14] M. Hamzaoui, A. Hadiouche, S. Tiachacht, Enhancing energy, exergy, and environment performances of ultra-low-temperature three-stage Cascade refrigeration cycle: optimization and comparative analysis, Arab. J. Sci. Eng. (2024) 1–29.

[15] Q. Wang, D. Su, X. Liu, L. Yao, J. Li, P. Wang, N. Zhang, Y. Yao, Comparative analysis of thermodynamic performance of three-stage cascade refrigeration system assisted with internal heat exchanger, Proceedings of Int. Conference on Appl. Energy (2020) 1–6. Paper ID 100.

[16] A. Mota-Babiloni, M. Mastani Joybari, J. Navarro-Esbrí, C. Mateu-Royo, Á. Barragán-Cervera, M. Amat-Albuixech, F. Molés, Ultralow-temperature refrigeration systems: configurations and refrigerants to reduce the environmental impact, Int. J. Refrig. 111 (2020) 147–158.

[17] S.A. Klein, Engineering Equation Solver, EES), Academic Professional Version F-Chart Software, Middleton, 2013.

[18] Z. Sun, Q. Wang, B. Dai, M. Wang, Z. Xie, Options of low global warming potential refrigerant group for a three-stage cascade refrigeration system, Int. J. Refrig. 100 (2019) 471–483.

[19] M.H. Nabil, Y. Khan, M.W. Faruque, M.M. Ehsan, Thermo-economic assessment of advanced triple cascade refrigeration system incorporating a flash tank and suction line heat exchanger, Energy Convers. Manag. 295 (2023) 117630.

[20] D. Sánchez, R. Cabello, R. Llopis, I. Arauzo, J. Catalán-Gil, E. Torrella, Energy performance evaluation of R1234yf, R1234ze (E), R600a, R290 and R152a as low-GWP R134a alternatives, Int. J. Refrig. 74 (2017) 269–282.

[21] O. Pektezel, S.N. Ozdemir, Performance optimization of new generation R290 and R1234yf refrigerants: a response surface methodology approach, Appl. Therm. Eng. 269 (2025) 125927.

[22] W. Ye, Y. Liu, Z. Zhou, L. Hu, Y. Liu, Performance prediction of an auto-cascade refrigeration system using multiple-algorithmic approaches, Energy 314 (2025) 134197.

[23] S.N. Ozdemir, I. Taymaz, F.G.B. San, E. Okumuş, Performance assessment and optimization of the PEM water electrolyzer by coupled response surface methodology and finite element modeling, Fuel 365 (2024) 131138.

[24] S. Silviana, F. Hermawan, J. Indracahya, D.A.L. Kusumawardhani, F. Dalanta, Optimizing the environmentally friendly silica-cellulose aerogel composite for acoustic insulation material derived from newspaper and geothermal solid waste using a central composite design, J. Sol-Gel Sci. Technol. 103 (2022) 226–243.
[25] M. Hoseini, S. Hamidi, E. Salehi, A. Mohammadi, F. Mirhoseini, M. Ravaghi, Multivariate multi-objective optimization of production conditions for electro-spun skin scaffold using RSM and investigation of gamma irradiation effects on the properties of the optimized sample, Heliyon 10 (2024).
[26] H. Ghaebi, E. Soleymani, Investigating the effect of parameters in the thermodynamic analysis of the solid oxide fuel cell cycle using response surface methodology, Sci. Rep. 15 (2025) 181.
[27] A.K. Choudhary, H. Pramanik, Optimization and validation of process parameters via RSM for minimizing use of resources to generate electricity from a DEFC, Int. J. Energy Res. 45 (2021) 20413–20429.
[28] M. Hamzaoui, S. Tiachacht, A. Hadiouche, Optimization of a three-stage cascade refrigeration system operating with natural refrigerants to produce low temperatures by applying a bio-inspired method, Thermal Sci. Eng. Progress 50 (2024).
[29] S. Ji, Z. Liu, J. Li, T. Wang, Thermodynamic analysis and performance optimization on an ultra-low-temperature cascade refrigeration system using refrigerants R290 and R170, Asia Pac. J. Chem. Eng. 20 (2025) e3179.
[30] S. Kumar, P. Gahlot, S. Kumar, A. Kumar, A novel ultra-low temperature cascade refrigeration with dual auxiliary loop to enhance thermal performance, Sci. Rep. 15 (2025) 23214.
[31] M. Hamzaoui, A. Grine, S. Tiachacht, H. Beltagy, Optimization of a liquid injection NH_3/CO_2 cascade refrigeration system, Energetic, Exergetic and Environ. Assess. Process Safety and Environ. Protection 196 (2025) 106862.
[32] M.M. Arefin, D. Mondal, M.A. Islam, Optimizing cascade refrigeration systems with low GWP refrigerants for low-temperature applications: a thermodynamic analysis, Energy Conversion and Manage: X 24 (2024) 100722.
[33] S. Kumar, P. Gahlot, S. Kumar, Energy, exergy and economical analysis of N2O based Cascade refrigeration system for ultralow temperature cooling applications using different eco-friendly refrigerants in high temperature cycle, Results Eng. 22 (2024) 102259.
[34] Z. Sun, Y.A. Wang, Comprehensive performance analysis of cascade refrigeration system with two-stage compression for industrial refrigeration, case studies, Therm. Eng. 39 (2022).
[35] M. Hamzaoui, Z. Aidoun, H. Nesreddine, S. Tiachacht, Optimisation of a cascade refrigeration system with natural refrigerants, based on nature-inspired algorithms, Arab. J. Sci. Eng. 49 (2024) 7701–7730.
[36] S. Ata, Comprehensive evaluation of a gas turbine-based multi-generation system for power, heating, cooling, freshwater, hydrogen and ammonia: 4E assessment and multi-objective optimization with RSM desirability approach, Renew. Energy 246 (2025) 122900.
[37] R. Govindasamy, S. Subramani, P.D. Kumar, Optimization of design and fuel parameters of a DI CI engine through desirability function and RSM for lower emissions and clean environment, J. Energy Inst. 114 (2024) 101607.